JOINT EUROPEAN TORUS

JET–P(89)10

M.J. Loughlin, P. van Belle, N.P. Hawkes, O.N. Jarvis,
G. Sadler, D.B. Syme and JET Team

Measurement of the Fractional Thermonuclear Neutron Yield during Deuterium Neutral-Beam Injection into Deuterium Plasmas

Measurement of the Fractional Thermonuclear Neutron Yield during Deuterium Neutral-Beam Injection into Deuterium Plasmas

M.J. Loughlin[1], P. van Belle, N.P. Hawkes[2], O.N. Jarvis,
G. Sadler, D.B. Syme and JET Team*

JET-Joint Undertaking, Culham Science Centre, OX14 3DB, Abingdon, UK

[1]Depart:nent of Physics, University of Birmingham, B15 21T, U.K.
[2]Harwell Laboratories, Harwell, Oxon, OXll ORA, U.K.
** See Appendix 1*

Preprint of Paper to be submitted for publication in
Nuclear Instruments and Methods

MEASUREMENT OF THE FRACTIONAL THERMONUCLEAR NEUTRON YIELD DURING DEUTERIUM NEUTRAL-BEAM INJECTION INTO DEUTERIUM PLASMAS

M J Loughlin*, P van Belle, N P Hawkes+, O N Jarvis,
G Sadler and D B Syme+

JET Joint Undertaking, Abingdon, Oxon, OX14 3EA, UK
* Department of Physics, University of Birmingham, B15 2TT, UK
+ Harwell Laboratories, Harwell, Oxon, OX11 ORA, UK

ABSTRACT

Two ^{3}He ionisation chambers were used at the Joint European Torus (JET) to measure neutron energy spectra for discharges in which deuterium neutral beams were injected into deuterium plasmas. By comparing the measured spectra with theoretical calculations, the fraction of the total neutron yield due to thermonuclear reactions was deduced. Calculated thermonuclear fractions agree well with the experimental results.

1. INTRODUCTION

The Joint European Torus (JET) is the largest operational fusion experiment and is supported by the European Communities through the organisation EURATOM. It is furnished with comprehensive plasma diagnostics instrumentation. Up to the present time, operation has been restricted to deuterium plasmas with neutron yields of up to 10^{16} neutrons/sec. It is obvious that neutron diagnostics have an essential role to play in such a machine. In particular, neutron spectrometry is uniquely capable of separating the contributions to the total neutron yield according to the reaction mechanisms responsible for their generation.

Earlier work in the field of neutron spectrometry as applied to magnetic fusion devices has, in some instances [1,2,3], demonstrated that the neutron production was of a non-thermal origin, whilst in others [4,5,6,7], it was able to confirm that the neutron production was indeed thermonuclear, in which case it sometimes proved possible [6,7,11a] to determine directly the central ion temperature in the plasma. Here, we present measurements of neutron spectra from JET plasmas

heated by the injection of powerful neutral deuterium beams (NBI), which results in the strong emission of 2.5 MeV neutrons due to reactions between the fast beam ions and the bulk deuterium ions of the plasma. The strong heating has the objective of raising the plasma temperature and, therefore, the neutron production rate from thermonuclear reactions is also increased. The neutron energy spectra take on a form which depends on the relative proportion of thermonuclear to beam-plasma neutron production; they are, accordingly, analysed to give the percentage thermonuclear yields. The analysis techniques have not been fully optimised yet, but the results give satisfactory agreement with theoretical predictions of both the neutron energy distributions and the fractional thermonuclear yields.

2. NEUTRON PRODUCTION DURING NBI

The total fusion neutron yield (Y_{tot}) during deuterium neutral-beam injection (NBI) can be separated into three components, thus:

$$Y_{tot} = Y_{pp} + Y_{bp} + Y_{bb} \qquad (1)$$

where Y_{pp} is the thermonuclear (plasma-plasma) yield, Y_{bp} is the beam-plasma yield and Y_{bb} is the beam-beam yield. For the circumstances of the measurements reported here, the beam-beam contribution can be shown to be negligible. Thus, the parameter of interest, namely the fractional plasma-plasma yield (F), is given by:

$$F = \frac{Y_{pp}}{Y_{pp} + Y_{bp}} \qquad (2)$$

The characteristics of the thermonuclear neutron production are well known. The energy spectrum is a Gaussian centred at 2.45 MeV with a full width at half-maximum (fwhm) given by:

$$\text{fwhm} = c\, T_i^{\frac{1}{2}} \qquad (3)$$

where c is weakly dependent on the ion temperature T_i and is often taken to be a constant (= 82.5 $\text{keV}^{\frac{1}{2}}$, T_i in keV) [10,11].

The calculation of the spectrum from a beam-heated plasma has been attempted by a number of authors [6,12,13,14]. Calculations have been performed specifically for JET, using the code FPS [11], in which the geometry of the neutral injectors and the lines-of-sight of the spectrometers (described in the next section) have been modelled. As opposed to calculations by other authors, the anisotropy of the cross-section was included. Some typical results are illustrated in figures 1a and 1b. A spectrum obtained with a detector viewing the plasma in a direction perpendicular to the magnetic field would show a bi-modal distribution. This arises because ions rotating around the field lines in a poloidal plane produce upward and downward energy shifts in the neutron energy spectrum as they move towards or away from the detector. The neutron spectrum emitted tangentially is a distorted gaussian shifted in energy either upwards or downwards for parallel or anti-parallel emission, due to the parallel motion of the beam ions. Thus, a detector with an arbitrary line-of-sight through the plasma will observe a bi-modal distribution (fig. 1a) which becomes increasingly symmetrical as the line-of-sight moves towards the perpendicular (fig. 1b). The detailed shape of the spectrum depends on a number of plasma parameters, including the energy and the direction at which the beams are injected, the ion temperature, the deuteron to electron density ratio (n_d/n_e), the plasma current, the plasma rotation and the line-of-sight. It should be remembered that any measurement of a spectrum will be the sum of beam-plasma and thermonuclear contributions, as in figures 1c and 1d.

A code, PENCIL [15], is used at JET to model the important aspects of neutral-beam injection. It can be used to provide information on fast ion deposition, electron or ion heating, beam driven current and momentum deposition, and the beam-plasma and thermonuclear neutron yields which are of particular interest to this work. The code can be used to analyse specific shots by accessing the JET database. However, because of the uncertainties in some of the relevant plasma parameters, the accuracy of the calculations is strictly limited. Specifically, the thermonuclear yield scales as $n_d^2\, T_i^4$ whereas the beam-plasma yield scales as $(n_d/n_e)T_e^{3/2}P_B$, where T_e is the electron temperature, and P_B is the injected beam power and n_d and n_e are the deuterium and electron densities respectively. The uncertainty in both T_i and T_e is about 10% and that in n_d/n_e is about 20% since the impurity content of the plasma is only known approximately. Thus, the accuracy of the thermonuclear yield calculation is typically ± 40%, that of the beam-plasma yield at best 25%.

Since the errors are correlated, the ratio F should be accurate to ± 40%. It should be noted that no neutron measurements are included as input to the PENCIL code.

In the present work, experimental measurements of the fractional thermonuclear yields were extracted from the spectrum shapes (by making use of the FPS calculations) and were compared with the predictions provided by PENCIL. It is implicit in this work that the conditions in the plasma centre can be taken as representative of the plasma as a whole with regard to the neutron emission. The PENCIL calculations support this assumption for the discharges to be studied here.

3. THE SPECTROMETERS

The two neutron spectrometers used in this work are ^{3}He ionisation chambers. Both are 'SEFORAD' fast neutron spectrometers [16], containing a mixture of ^{3}He, argon, and methane at a pressure of approximately 10 bar. The ion chamber collects the charge produced by the triton and the proton from each ^{3}He(n,p)T reaction. The resolution of this device to (mono-energetic) 2.5 MeV neutrons is 40 keV and the response function between 2 and 3 MeV has been the subject of detailed measurements. It can be represented as the sum of two Gaussians and an error function. Seven parameters are required to define this response function, most of these varying with incident neutron energy. Full details will be reported separately [17]. The full response (0-3 MeV) of these detectors to mono-energetic neutrons is complex (see figure 2). This is because of incomplete charge collection (wall effect) and elastic scattering from ^{3}He and H. The very high sensitivity of the detector to thermal neutrons, and the (moderate) sensitivity to γ-rays together with long charge collection times ($\geq$ 6 μsec), limit the useful count-rate; at count-rates in excess of 4000 counts per second the spectrum is distorted by pile-up. We have shown that for lower rates pile-up distortion is negligible compared to the estimated statistical errors.

As discussed above, the neutron spectra from beam-heated plasmas can emphasise different physical phenomena according to the viewing direction. In order to exploit this feature, two lines-of-sight have been provided for the ^{3}He spectrometers. The first detector is sited in the roof laboratory above the torus and over a penetration through the floor. This provides the detector with a well collimated vertical line-of-sight through the centre of the plasma, at a

position approximately 20 m from the horizontal mid-plane (figure 3). The second spectrometer is positioned inside a massive hydrogenous shield in the torus hall about 15 m from the plasma centre (figure 4) [18]. This shielding provides the ion chamber with a line-of-sight in the mid-plane of the vacuum vessel (at 60° to the magnetic field) aligned so as to avoid the central column of the machine. The enclosure shields the chamber from the general background, especially thermal and epi-thermal neutrons to which it is extremely sensitive. Only the full energy peak is of value in determining the neutron spectrum. With this shielding, the number of events in the full energy peak was maximised at 1/20th of the total number of counts in the entire spectrum. This means that the maximum 'useful' count-rate is only 200 cps and, since approximately 800 counts were required for an unfolding, a minimum of 4 plasma-seconds is required to accumulate a spectrum. Both detectors view the plasma through specially thinned closure plates fitted to the diagnostic ports in the vacuum vessel. Because of the magnet coils and neutron shielding around the rest of the vessel, the neutron flux emerges predominantly through these 'viewing' ports. The combination of collimation, carefully chosen line-of-sight and the thin material over the ports results in negligible scattered flux and spectrum degradation for either line-of-sight.

Pulses from the detector enter the attached pre-amplifier, and are then sent to an ORTEC 673 amplifier and an ORTEC 542 linear gate and stretcher. For the torus hall instrument, there is a 120 m length of superscreened cable connecting the pre-amplifier with the electronics in the diagnostic hall. The linear gate and stretcher is used to shape the pulses before they are sent to a LeCroy 3512 analogue-to-digital converter and a LeCroy 3588 histogramming memory from which the data are collected by the JET computer operated data acquisition system (CODAS [19]). A series of neutron spectra is automatically recorded for each shot. Each spectrum is accumulated during a one second 'time slice' into 256 channels; up to 20 spectra are obtained for each discharge. Precision pulse generators (ORTEC 448) are used to monitor the resolution of the spectrometers. The positions of the thermal neutron peak and the 2.45 MeV peak produced during Ohmic discharges were used to calibrate the spectrometers assuming a linear energy scale.

4. THE ANALYSIS OF THE PULSE-HEIGHT SPECTRA

The pulse height spectra were unfolded using a program (EDRF) specifically written for this purpose [17]. The measured spectrum, M(E), is described by equation 4:

$$M(E) = \int_{-\infty}^{\infty} R(E,E')f(E')dE' \qquad (4)$$

where R(E,E′) is the response function of the detector, ie. neutrons in the energy range E′ to E′ + dE′ have a probability R of producing a pulse of height E. The response function is described by the sum of two Gaussians and a 'wall effect' function [17]; figure 5 shows the response to mono-energetic 2.5 MeV neutrons. A full energy-dependent response function is included in the code. The incident neutron spectrum, f(E′), is described by a histogram, $H(E_i)$, made up of a number of equal width bins; no assumptions are made about the shape of f(E′) except that its total width is 800 keV, extending from 2.05 MeV to 2.85 MeV. A 'first guess' is made of the incident neutron spectrum and a theoretical pulse height spectrum, $M_T(E)$, is calculated using an approximate form of equation 4, thus:

$$M_T(E) = \sum_{i=n_1}^{n_2} R(E,E_i)\ H(E_i) \qquad (5)$$

The index i refers to the channel number in the fitting region. $R(E,E_i)$ is the response to neutrons of energy E_i and $H(E_i)$ is the bin height of the incident neutron spectrum at energy E_i. The values of $H(E_i)$ are varied until the fit of M_T to the measured spectrum is optimised. The optimisation is achieved by the minimisation of χ^2, using the Harwell subroutine VA02A [20] and the errors on the heights of each bin are found using the subroutine SV10A [20]. Eleven bins were used to describe f(E′) as a compromise between maintaining the resolution of the unfolded neutron spectrum and keeping the number of fitting parameters to a minimum. Figure 6 shows an example of an unfolded neutron spectrum and the corresponding fit to the raw data.

A second program (BPPP) was written to calculate F (equation 2) from the unfolded neutron spectrum. An appropriate beam-plasma spectrum, corresponding to the correct line-of-sight, is taken from previous FSPEC calculations. This

is regarded as a 'typical' spectrum and its shape is not altered, only the relative magnitude is changed. Next, a Gaussian neutron spectrum is generated with a width appropriate to a particular ion temperature using equation 3. The beam-plasma and the thermonuclear spectra are then summed and binned into a histogram of the same width and number of bins as the unfolded experimental neutron spectrum. By varying the heights of the two spectra and the ion temperature, a best fit is obtained and F is calculated.

Beam-heating has been applied for periods of 4 seconds or less. As the dynamic range of the detector is limited, and a time-resolution of one second is required, spectra from a number of shots must be added together to provide enough counts for a successful unfolding. The selection of shots that were sufficiently alike to allow summation was a complex and time consuming process. Ideally, only data from identical shots should be summed before unfolding. If this is not the case any information contained in the shape of the spectrum may well be lost. This averaging was kept to a minimum compatible with obtaining good statistics.

Similar discharges were selected using a standard procedure. Initially, shots were selected with the same plasma current, magnetic field configuration and methods of additional heating. They were then examined more closely using the neutron yield monitor [18] (see figure 7). The deuterium reaction-rate as a function of time was examined for a number of shots and those with dissimilar yields were eliminated. This was usually sufficient to identify similar shots; however, the survey of other relevant plasma parameters was continued to ensure that there were no large dissimilarities. (This included an examination of the ion temperature, the electron density, and the neutral-beam and RF power levels).

Eight series of shots were judged to be sufficiently similar to allow summation. These are listed in table 1, along with some of the relevant plasma parameters. The series are labelled A to H. It should be noted that the shots making up series B have different timings but were identical in all other respects; these spectra were integrated over the time period from 12 to 16 seconds into the shot to include the periods of high neutron yield from all the shots in this series.

5. RESULTS

The codes EDRF and BPPP were used to analyse the spectra for each series. Individual time slices were analysed when there were enough counts in the summed spectra (except in the case of series B, discussed above). The following points were noted about the general shape of each spectrum. Firstly, as predicted, the neutron energy spectrum is broader than that produced during purely Ohmic heating and is distinctly non-Gaussian. Figure 8 compares a Gaussian spectrum from a 3 keV plasma with the unfolded spectrum from series B (torus hall line-of-sight); the response of the spectrometer to mono-energetic neutrons is also shown. This broadening is quite clear. Secondly, the unfolded spectrum is peaked and does not show the characteristic double-humped shape of pure beam-plasma reactions. This clearly indicates that a large proportion of the total neutron yield is due to plasma-plasma interactions. The code BPPP was used to estimate this proportion. Fair agreement between the unfolded spectrum and the FPS predictions could be obtained, as described below.

With the ion temperature and F as free variables, the fits of the spectra obtained with the detector in the roof laboratory yielded values for the ion temperature which were consistent with estimates obtained from other diagnostics. However, reasonable fits to the torus hall spectra could only be obtained after including a neutron spectrum which arises from a population of fast deuterons streaming in the opposite direction to their direction of injection (figure 9). This phenomenon is expected in tokamaks in which a fraction of the injected particles become trapped in orbits so that they oscillate toroidally (magnetic mirror trapping). The trapped particles do not affect the spectra obtained with the roof laboratory spectrometer. To obtain a satisfactory fit to the spectra obtained with the torus hall spectrometer (figure 10), with the ion temperature fixed to the values obtained from the x-ray crystal spectrometer [21], it was necessary to assumed a 25% fraction of counter-streaming ions. The deduced values of F were then found to be generally consistent between both spectrometers and the PENCIL predictions (see Table 2). Thus the detailed shapes of the spectra are believed to be well understood. On the whole, the good agreement between measured and PENCIL values for F is rather surprising because PENCIL generally overpredicts the total neutron yields by a factor of 2 or more.

6. DISCUSSION

Figure 10 illustrates the fair agreement between the FPS calculations and the experimental measurements. In future, specific FPS calculations will be performed for selected shots and improved agreement can be expected. It may be possible to deduce the thermonuclear fraction using a spectrometer in the roof laboratory and using that information to deduce the trapped fraction using the torus hall spectrometer.

If all the relevant parameters (n_d, T_i, impurity content etc) were accurately known it would be thought possible to calculate the ratio F without reference to neutron spectra. Many problems exist, however. In particular, as discussed earlier, some of the important plasma parameters are not known at all well, with the ratio n_d/n_e in particular being unreliable for discharges with high impurity content. In this context, measurements of F by spectrometry should be of greater value in limiting the permitted values for T_i and n_d/n_e, especially when the analysis of the spectra is complemented by the use of the absolute neutron yield as a further constraint. An example of the power of this technique is afforded by the first analysis of slice 14 of series A which yielded F = .25 and an ion temperature of 1.3 keV ($\chi^2 = 2.0$); when however, the ion temperature was fixed to 4 keV, as given by the crystal spectrometer, F was found to be .30 ($\chi^2 = 2.4$). Both values for F are consistent to within the errors and agree with the PENCIL calculation of .30 ± .12. However, for a given deuteron density the first case (1.3 keV) predicts a total neutron yield 20 times lower than the second (4.0 keV). The combination of measurements thus constrain the n_d/n_e ratio to within narrow limits.

7. CONCLUSIONS

The measurement of neutron spectra during the injection of deuterium beams has provided an opportunity to measure the relative yields of the beam-plasma and plasma-plasma reactions and the success of this preliminary analysis justifies optimism in the techniques of neutron spectrometry and provides an incentive to refine them further. The spectrum measurements show convincingly the effect whereby the addition of powerful neutral beam heating (which instantly raises the neutron emission by more than one order of magnitude) also has the (more

gradual) effect of heating the plasma such that the thermal emission grows to a level comparable with the beam-induced emission. It has been demonstrated that the fractional plasma-plasma yield F and the trapped ion fraction can be obtained from the shape of the neutron spectra with useful accuracy even though the ion temperature is known only approximately. With improved statistical accuracy in the measured spectra, there is reason to expect that ion temperature, F and the trapped ion fraction can be derived simultaneously. Provided the ion temperature is known, by whatever means, the deuterium plasma density can be derived with the additional constraint provide by the measured total neutron yield. Neutron spectrometry thus offers the possibility of enhancing our understanding of neutron beam heated discharges in tokamaks.

8. ACKNOWLEDGEMENTS

This work was only made possible by the combined efforts of the entire JET team; in particular, we are grateful to Dr D Muir for providing the specific PENCIL predictions needed for comparison with our measurements.

Part of this work was performed while one of us (MJL) was studying for the degree of Doctor of Philosophy at Birmingham University. He would like to thank his supervisors, Prof J Walker and Dr K Randle for their assistance during this time, and to the UKAEA for providing financial support.

REFERENCES

[1] B Rose, A E Taylor and E Wood, Nature 181 (1958) 1630.
[2] R A Coombe and B A Ward, Plasma Phys 5 (1963) 273.
[3] F Pecorella et al, Phys Fluids 20 (1977) 675.
[4] G L Morgan and A C England, Nucl Instrum Meth 129 (1975) 1.
[5] M Brusati et al, Nucl Fusion 18 (1978) 1205.
[6] W Fisher, Thesis, MIT (1983).
[7] O N Jarvis et al, Rev Sci Instrum 57 (1986) 626.
[8] J D Strachan et al, Nature 279 (1979) 626.
[9] K Hübner, R Bätzner, H Hinsch, 12th European Conference on Controlled Fusion and Plasma Physics, Budapest, 1986.
[10] H Brysk, Plasma Phys 15 (1973) 611.
[11] a) G Sadler and P van Belle, 13th European Conference on Controlled Fusion and Plasma Heating, Schliersee, 1986.

b) P van Belle and G Sadler, in Basic Advanced Fusion Plasma Diagnostic Techniques (Varenna, 1986), Vol III, EUR 10797 EN.

[12] G Lehner and F Pohl, Zeischrift fur Physik 207 (1976) 83.

[13] J Scheffel, Nucl Instrum Meth 221 (1984) 449.

[14] D R Slaughter, Rev Sci Instrum 57 (1986) 1751.

[15] P M Stubberfield and M L Watkins, JET Internal Report, DPA(06)/87(1987).

[16] S Shalev and J M Cuttler, Nuclear Science Eng 51 (1973) 52.

[17] M J Loughlin, PhD Thesis, Birmingham University, 1988 and to be published.

[18] E W Lees et al, Radiation Effects 95 (1986) 1259.

[19] E Jones, Nucl Instrum Meth A247 (1986) 58.

[20] A R Curtis and M J D Powell, Computer Journal 8 (1965) 358.

[21] R Giannella, F Bombarda, E Kallne, L Panaccione and G Tallents, Bull Am Phys Soc 31 (1986) 1590.

Series	Shot Numbers	Plasma Current (MA)	Magnetic Field (Tesla)	NBI Power (MW)	RF Power (MW)
A	10759 10761 10762 10763 10764 10766	2.0	2.2	7.3	2.0
B	10789 10793 10794	3.0	2.2	9.3	0.0
C	10808 10818 10819 10823	3.0	2.2	7.1	0.0
D	10809 10810 10816 10817	3.4	2.2	9.1	0.0
E	10851 10854	2.0	2.2	7.2	0.0
F	10943 10944 10945 10954	5.0	3.4	7.4	0.23
G	10946 10947 10948 10949	5.0	3.4	5.0	0.85
H	10974 10976 10977 10979	5.0	3.4	7.9	1.7

Table 1: The shots summed in making up series A to H, the plasma current, the toroidal magnetic field and the additional heating powers. At these levels (≤2MW), the RF heating has very little effect in comparison with the neutral beam heating.

Series	Time Slices	X-Ray Ion Temp (keV)	F TH	F RL	PENCIL calculation
A	13	4	.1	.2	.2±.1
A	14	4	.2	.25	.3±.2
B	12-16	5	.3	.4	.4±.2
C	11-12	4	.4	.3	.3±.1
C	13	4	.4	.4	.4±.1
C	14	4	.8	.4	.5±.1
D	11-12	6	.45	.4	.4±.2
D	13	6	.3	.25	.3±.1
D	14	6	.3	.3	.3±.1
E	11-12	7	.0	.25	.2±.1
E	13-14	6	.7	.3	.3±.1
F	8	6	.4	.3	.4±.1
F	9	6	.2	.7	.4±.2
F	10-11	5	.5	.4	.3±.1
G	9-11	5	.3	.6	.3±.1
H	9-10	6	.5	.4	.3±.1

Table 2: The plasma-plasma to total neutron yield ratio (F) deduced from the fit for the roof laboratory (RL) and torus hall (TH) detectors (including effect of 50% trapped particles). Also shown are the approximate ion temperatures from the X-ray diagnostic and the PENCIL results. The PENCIL predictions for F have an associated uncertainty of at least ±40%, resulting mainly from the ±10% uncertainty attributed to T_i. The accuracy of the experimental values is ± .1.

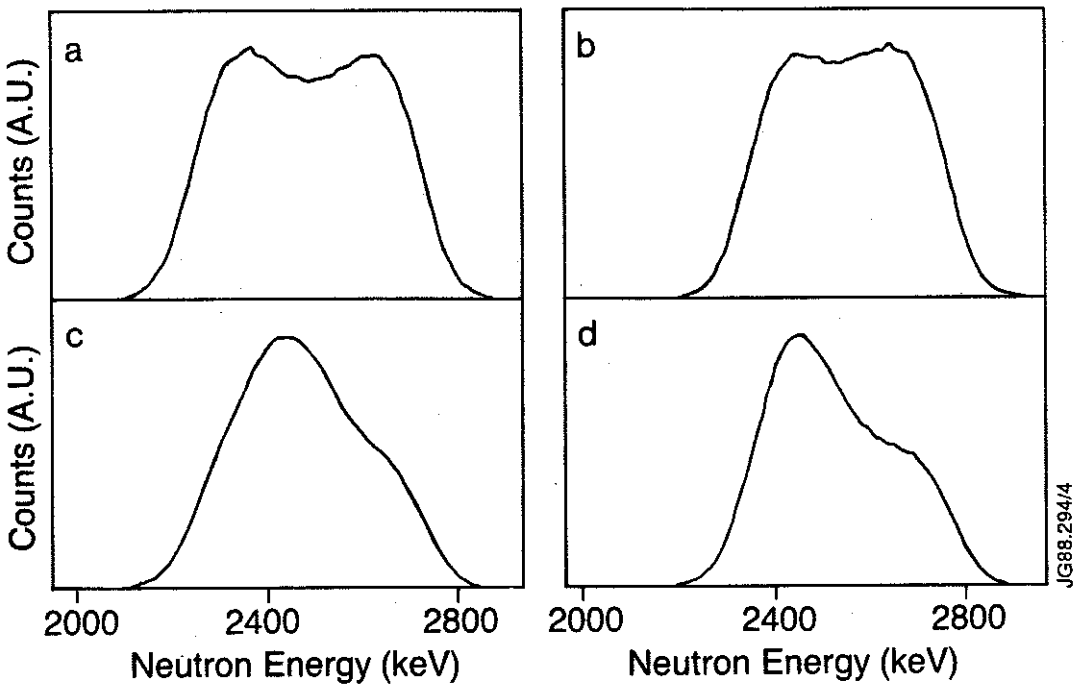

Fig. 1 FPS calculations of the beam-plasma spectrum.
a) Roof laboratory line-of-sight.
b) Torus hall line-of-sight.
c) Beam-plasma spectrum plus 25% plasma-plasma ($T_i = 6$ keV, roof laboratory).
d) Beam-plasma plus 25% plasma-plasma ($T_i = 6$ keV, torus hall).

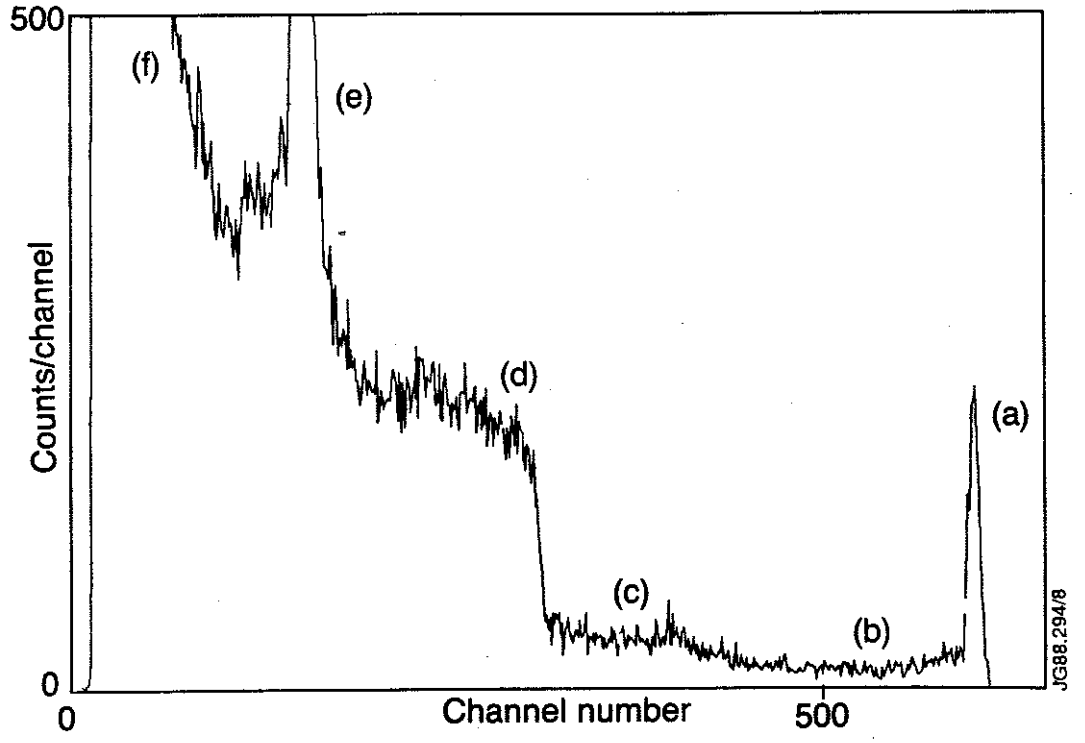

Fig. 2 Response function of ^{3}He ionisation chamber to mono-energetic neutrons.
a) full energy peak,
b) wall effect,
c) proton recoil events,
d) ^{3}He recoil events,
e) the thermal peak,
f) low pulse height events due to γ-rays.

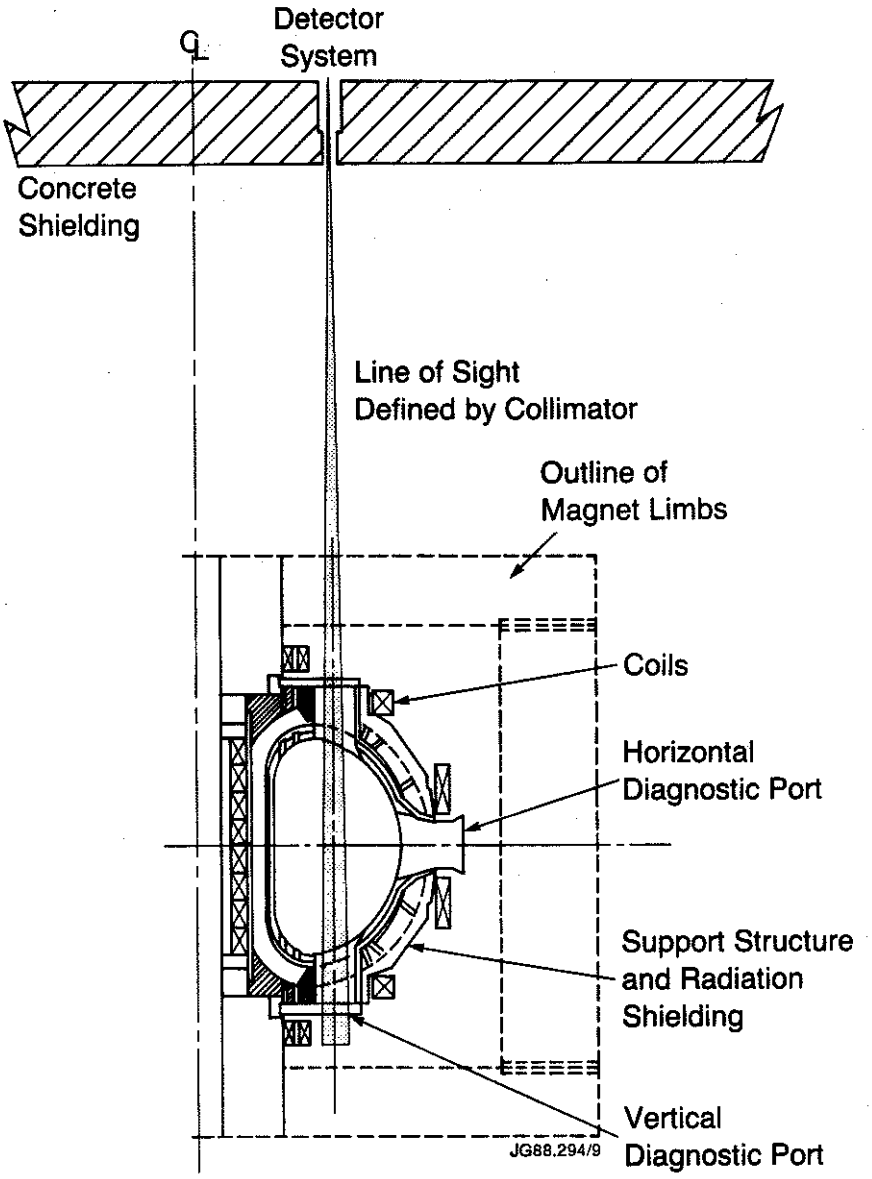

Fig. 3 The line-of-sight of the spectrometer positioned in the roof laboratory.

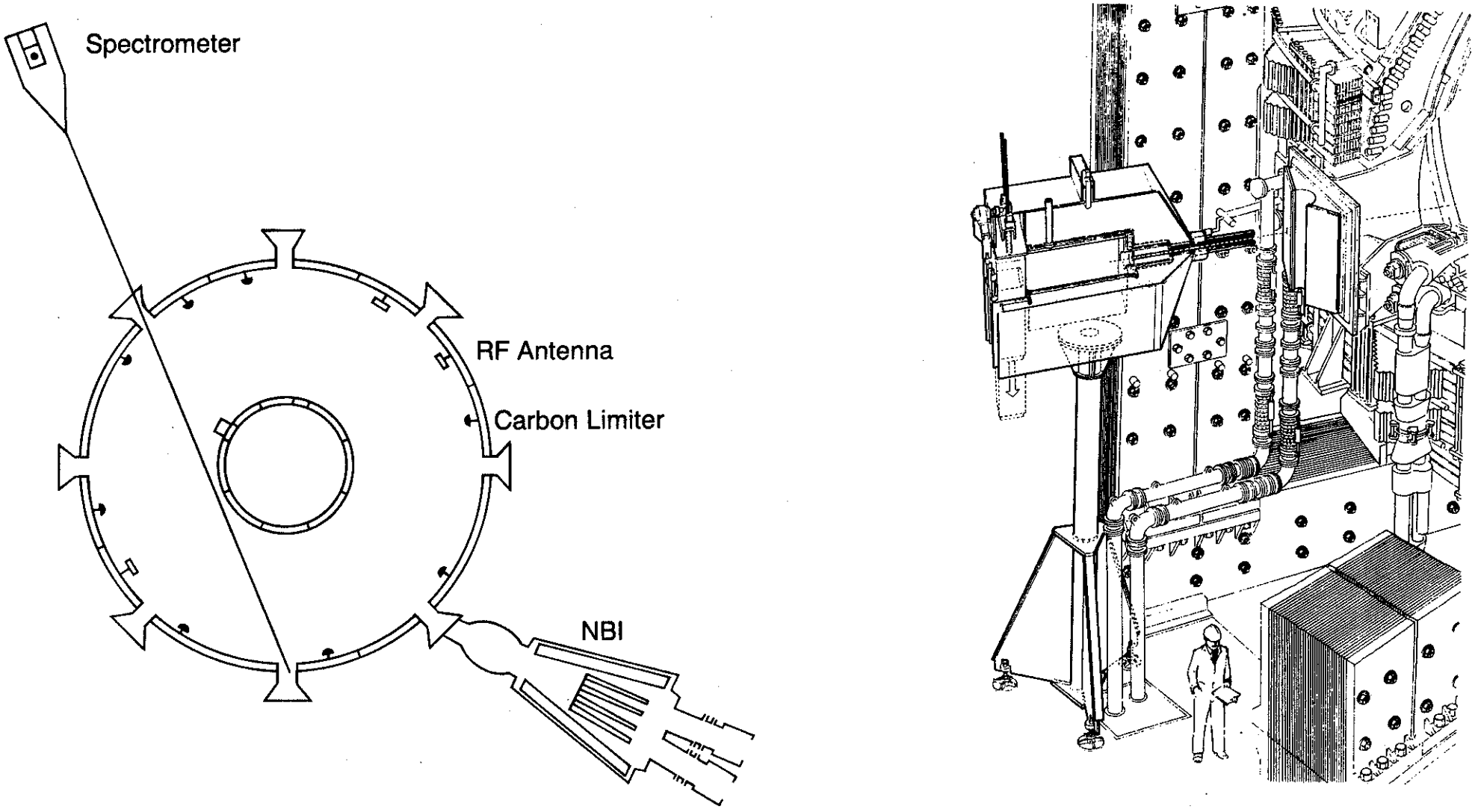

Fig. 4 The line-of-sight of the spectrometer in the torus hall (left) and the shielding for the spectrometer showing its position with respect to the viewing port (right).

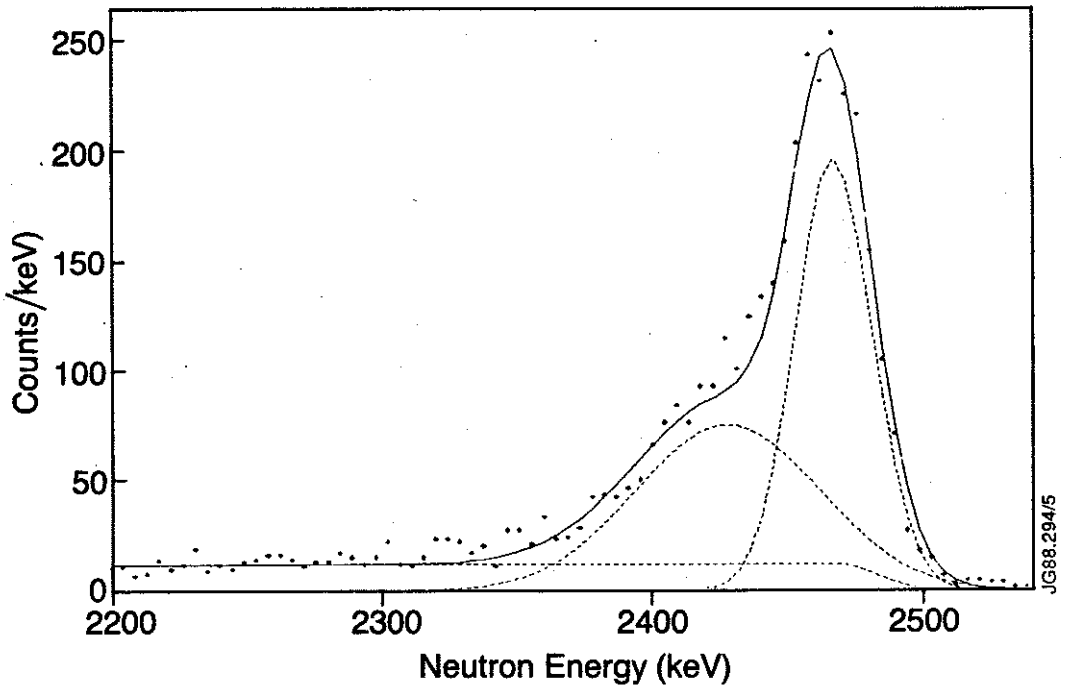

Fig. 5 The measured response function to 2.5 MeV neutrons (●), the fit (———), and the components of the fitting function (— — —).

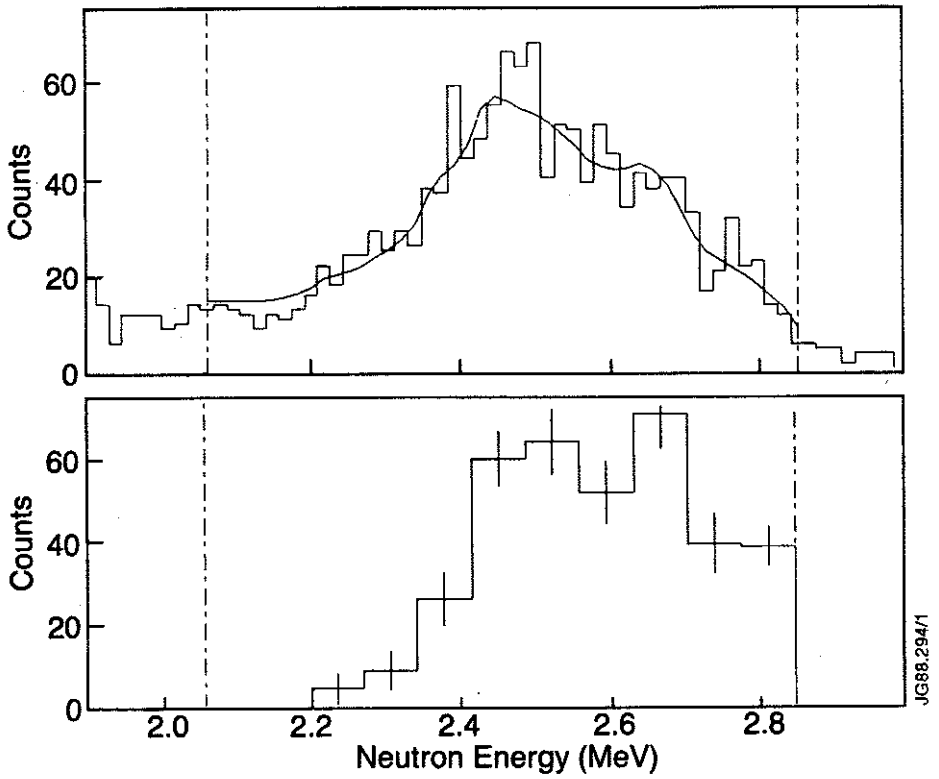

Fig. 6 The unfolded neutron spectrum calculated by EDRF (lower), and the corresponding fit (full line) to the original pulse-height spectrum (histogram) (upper).

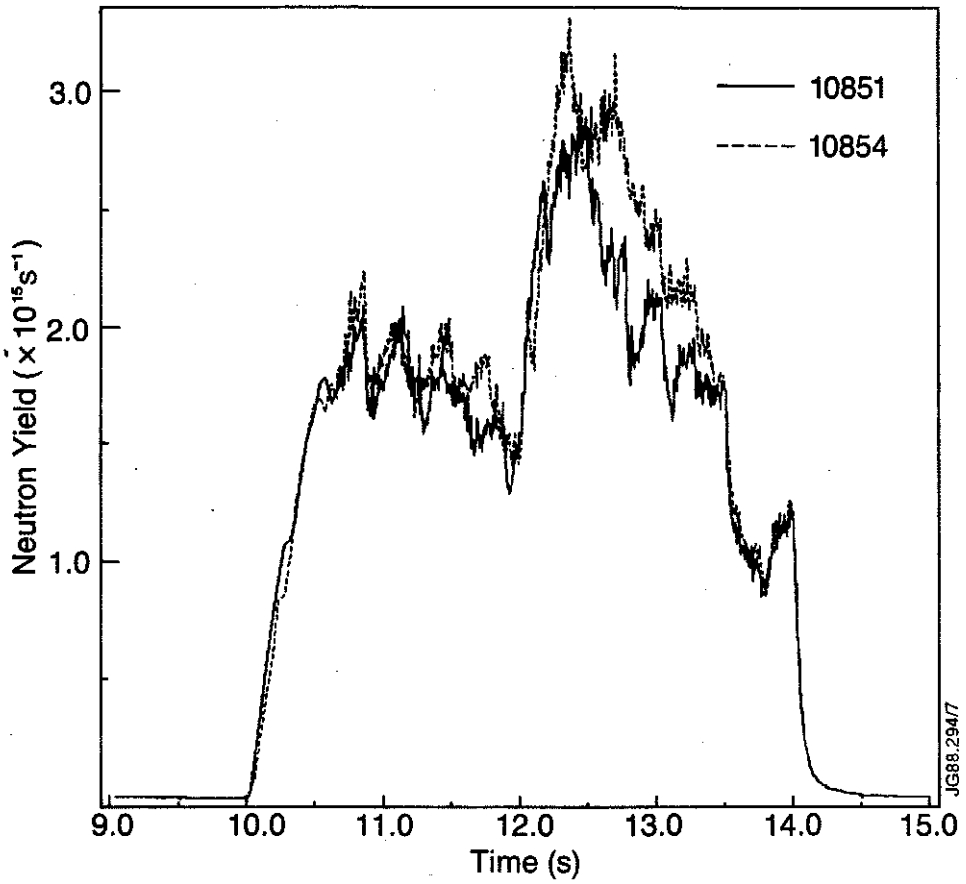

Fig. 7 The neutron production as a function of time for the shots making up series E.

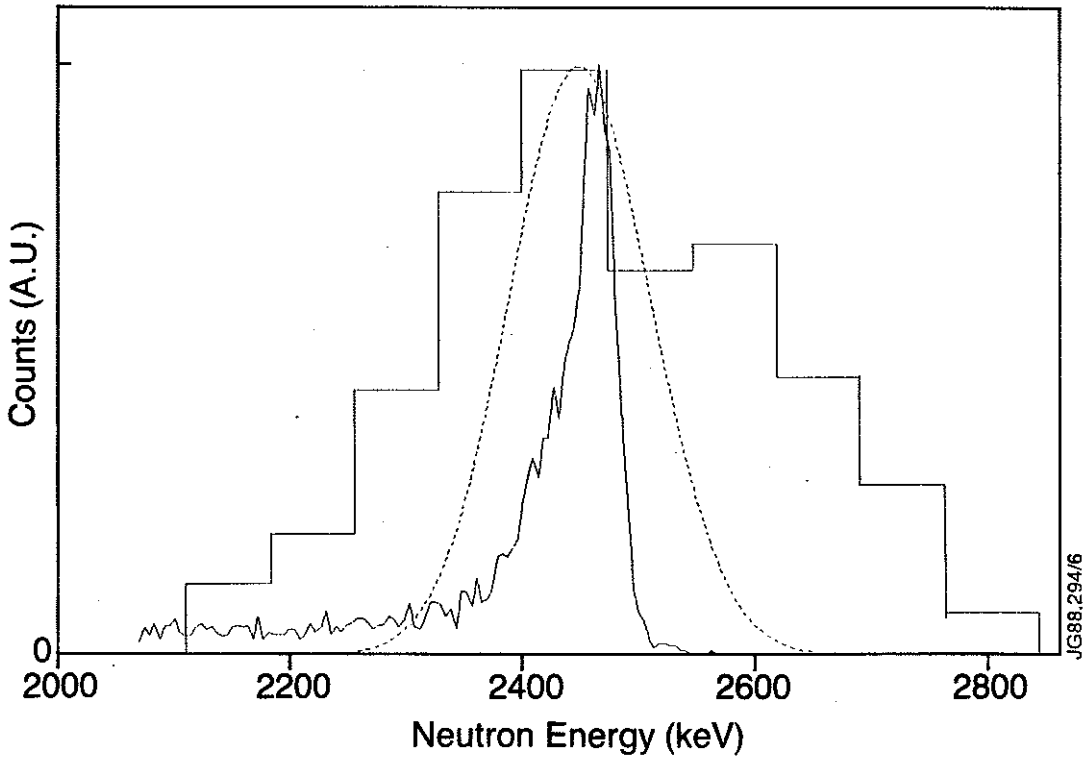

Fig. 8 The unfolded neutron spectrum from series B(TH) (histogram), the Gaussian (– – – –) produced by a Maxwellian plasma ($T_i = 3$ keV), and the measured response function (———).

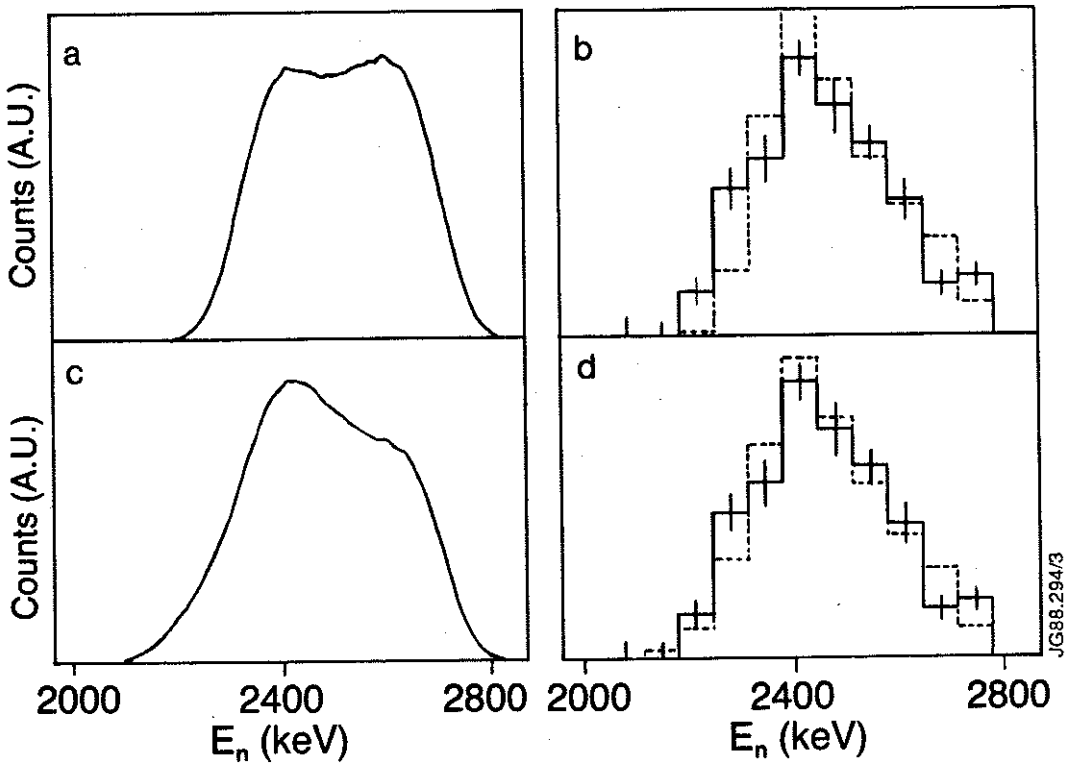

Fig. 9 FPS calculations of neutron spectra without (a) and with (c) counter-streaming ions, and corresponding comparison with the unfolded spectrum (b and d respectively). Solid histogram: unfolded spectrum. Dotted histogram: binned version of a and c, with thermonuclear component added. Error bars appropriate to counting statistics are shown on the unfolded spectra.

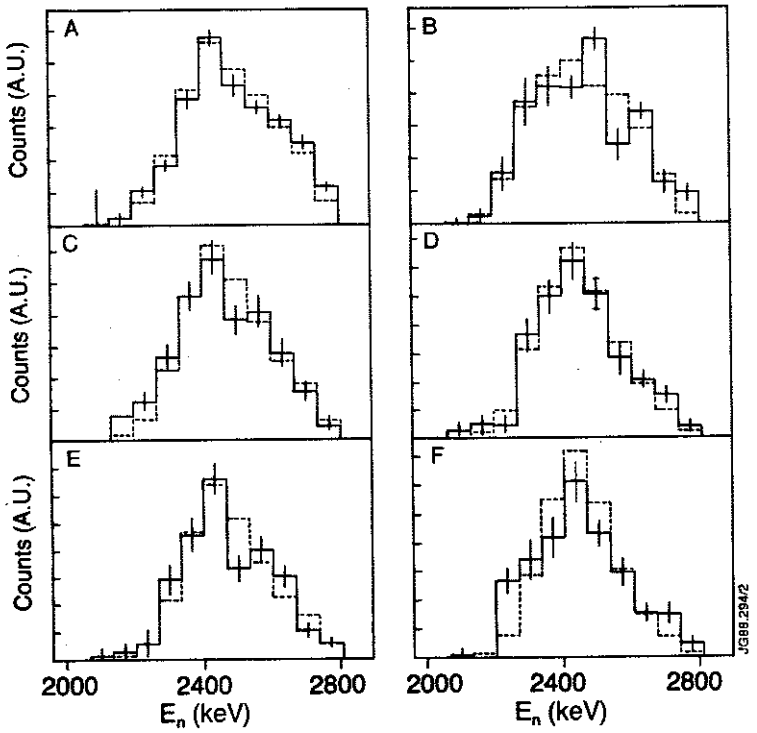

Fig. 10 Unfolded neutron spectra from each detector.
a) Series A, slice 14, torus hall.
b) Series A, slice 14, roof laboratory.
c) Series B, torus hall.
d) Series B, roof laboratory.
e) Series G, torus hall.
f) Series G, roof laboratory.
Solid histogram: Unfolded spectrum
Dotted histogram: Binned beam-plasma spectrum plus thermonuclear component.

APPENDIX 1.

THE JET TEAM

JET Joint Undertaking, Abingdon, Oxon, OX14 3EA, U.K.

J.M.Adams[1], F.Alladio[4], H.Altmann, R.J.Anderson, G.Appruzzese, W.Bailey, B.Balet, D.V.Bartlett, L.R.Baylor[24], K.Behringer, A.C.Bell, P.Bertoldi, E.Bertolini, V.Bhatnagar, R.J.Bickerton, A.Boileau[3], T.Bonicelli, S.J.Booth, G.Bosia, M.Botman, D.Boyd[31], H.Brelen, H.Brinkschulte, M.Brusati, T.Budd, M.Bures, T.Businaro[4], H.Buttgereit, D.Cacaut, C.Caldwell-Nichols, D.J.Campbell, P.Card, J.Carwardine, G.Celentano, P.Chabert[27], C.D.Challis, A.Cheetham, J.Christiansen, C.Christodoulopoulos, P.Chuilon, R.Claesen, S.Clement[30], J.P.Coad, P.Colestock[6], S.Conroy[13], M.Cooke, S.Cooper, J.G.Cordey, W.Core, S.Corti, A.E.Costley, G.Cottrell, M.Cox[7], P.Cripwell[13], F.Crisanti[4], D.Cross, H.de Blank[16], J.de Haas[16], L.de Kock, E.Deksnis, G.B.Denne, G.Deschamps, G.Devillars, K.J.Dietz, J.Dobbing, S.E.Dorling, P.G.Doyle, D.F.Düchs, H.Duquenoy, A.Edwards, J.Ehrenberg[14], T.Elevant[12], W.Engelhardt, S.K.Erents[7], L.G.Eriksonn[5], M.Evrard[2], H.Falter, D.Flory, M.Forrest[7], C.Froger, K.Fullard, M.Gadeberg[11], A.Galetsas, R.Galvao[8], A.Gibson, R.D.Gill, A.Gondhalekar, C.Gordon, G.Gorini, C.Gormezano, N.A.Gottardi, C.Gowers, B.J.Green, F.S.Griph, M.Gryzinski[26], R.Haange, G.Hammett[6], W.Han[9], C.J.Hancock, P.J.Harbour, N.C.Hawkes[7], P.Haynes[7], T.Hellsten, J.L.Hemmerich, R.Hemsworth, R.F.Herzog, K.Hirsch[14], J.Hoekzema, W.A.Houlberg[24], J.How, M.Huart, A.Hubbard, T.P.Hughes[32], M.Hugon, M.Huguet, J.Jacquinot, O.N.Jarvis, T.C.Jernigan[24], E.Joffrin, E.M.Jones, L.P.D.F.Jones, T.T.C.Jones, J.Källne, A.Kaye, B.E.Keen, M.Keilhacker, G.J.Kelly, A.Khare[15], S.Knowlton, A.Konstantellos, M.Kovanen[21], P.Kupschus, P.Lallia, J.R.Last, L.Lauro-Taroni, M.Laux[33], K.Lawson[7], E.Lazzaro, M.Lennholm, X.Litaudon, P.Lomas, M.Lorentz-Gottardi[2], C.Lowry, G.Magyar, D.Maisonnier, M.Malacarne, V.Marchese, P.Massmann, L.McCarthy[28], G.McCracken[7], P.Mendonca, P.Meriguet, P.Micozzi[4], S.F.Mills, P.Millward, S.L.Milora[24], A.Moissonnier, P.L.Mondino, D.Moreau[17], P.Morgan, H.Morsi[14], G.Murphy, M.F.Nave, M.Newman, L.Nickesson, P.Nielsen, P.Noll, W.Obert, D.O'Brien, J.O'Rourke, M.G.Pacco-Düchs, M.Pain, S.Papastergiou, D.Pasini[20], M.Paume[27], N.Peacock[7], D.Pearson[13], F.Pegoraro, M.Pick, S.Pitcher[7], J.Plancoulaine, J-P.Poffé, F.Porcelli, R.Prentice, T.Raimondi, J.Ramette[17], J.M.Rax[27], C.Raymond, P-H.Rebut, J.Removille, F.Rimini, D.Robinson[7], A.Rolfe, R.T.Ross, L.Rossi, G.Rupprecht[14], R.Rushton, P.Rutter, H.C.Sack, G.Sadler, N.Salmon[13], H.Salzmann[14], A.Santagiustina, D.Schissel[25], P.H.Schild, M.Schmid, G.Schmidt[6], R.L.Shaw, A.Sibley, R.Simonini, J.Sips[16], P.Smeulders, J.Snipes, S.Sommers, L.Sonnerup, K.Sonnenberg, M.Stamp, P.Stangeby[19], D.Start, C.A.Steed, D.Stork, P.E.Stott, T.E.Stringer, D.Stubberfield, T.Sugie[18], D.Summers, H.Summers[20], J.Taboda-Duarte[22], J.Tagle[30], H.Tamnen, A.Tanga, A.Taroni, C.Tebaldi[23], A.Tesini, P.R.Thomas, E.Thompson, K.Thomsen[11], P.Trevalion, M.Tschudin, B.Tubbing, K.Uchino[29], E.Usselmann, H.van der Beken, M.von Hellermann, T.Wade, C.Walker, B.A.Wallander, M.Walravens, K.Walter, D.Ward, M.L.Watkins, J.Wesson, D.H.Wheeler, J.Wilks, U.Willen[12], D.Wilson, T.Winkel, C.Woodward, M.Wykes, I.D.Young, L.Zannelli, M.Zarnstorff[6], D.Zasche[14], J.W.Zwart.

PERMANENT ADDRESS

1. UKAEA, Harwell, Oxon. UK.
2. EUR-EB Association, LPP-ERM/KMS, B-1040 Brussels, Belgium.
3. Institute National des Récherches Scientifique, Quebec, Canada.
4. ENEA-CENTRO Di Frascati, I-00044 Frascati, Roma, Italy.
5. Chalmers University of Technology, Göteborg, Sweden.
6. Princeton Plasma Physics Laboratory, New Jersey, USA.
7. UKAEA Culham Laboratory, Abingdon, Oxon. UK.
8. Plasma Physics Laboratory, Space Research Institute, Sao José dos Campos, Brazil.
9. Institute of Mathematics, University of Oxford, UK.
10. CRPP/EPFL, 21 Avenue des Bains, CH-1007 Lausanne, Switzerland.
11. Risø National Laboratory, DK-4000 Roskilde, Denmark.
12. Swedish Energy Research Commission, S-10072 Stockholm, Sweden.
13. Imperial College of Science and Technology, University of London, UK.
14. Max Planck Institut für Plasmaphysik, D-8046 Garching bei München, FRG.
15. Institute for Plasma Research, Gandhinagar Bhat Gujat, India.
16. FOM Instituut voor Plasmafysica, 3430 Be Nieuwegein, The Netherlands.
17. Commissiariat à L'Energie Atomique, F-92260 Fontenay-aux-Roses, France.
18. JAERI, Tokai Research Establishment, Tokai-Mura, Naka-Gun, Japan.
19. Institute for Aerospace Studies, University of Toronto, Downsview, Ontario, Canada.
20. University of Strathclyde, Glasgow, G4 ONG, U.K.
21. Nuclear Engineering Laboratory, Lapeenranta University, Finland.
22. JNICT, Lisboa, Portugal.
23. Department of Mathematics, Univeristy of Bologna, Italy.
24. Oak Ridge National Laboratory, Oak Ridge, Tenn., USA.
25. G.A. Technologies, San Diego, California, USA.
26. Institute for Nuclear Studies, Swierk, Poland.
27. Commissiariat à l'Energie Atomique, Cadarache, France.
28. School of Physical Sciences, Flinders University of South Australia, South Australia SO42.
29. Kyushi University, Kasagu Fukuoka, Japan.
30. Centro de Investigaciones Energeticas Medioambientales y Techalogicas, Spain.
31. University of Maryland, College Park, Maryland, USA.
32. University of Essex, Colchester, UK.
33. Akademie de Wissenschaften, Berlin, DDR.

CR 88.49.1A